Diamond Nitrogen Vacancy Research

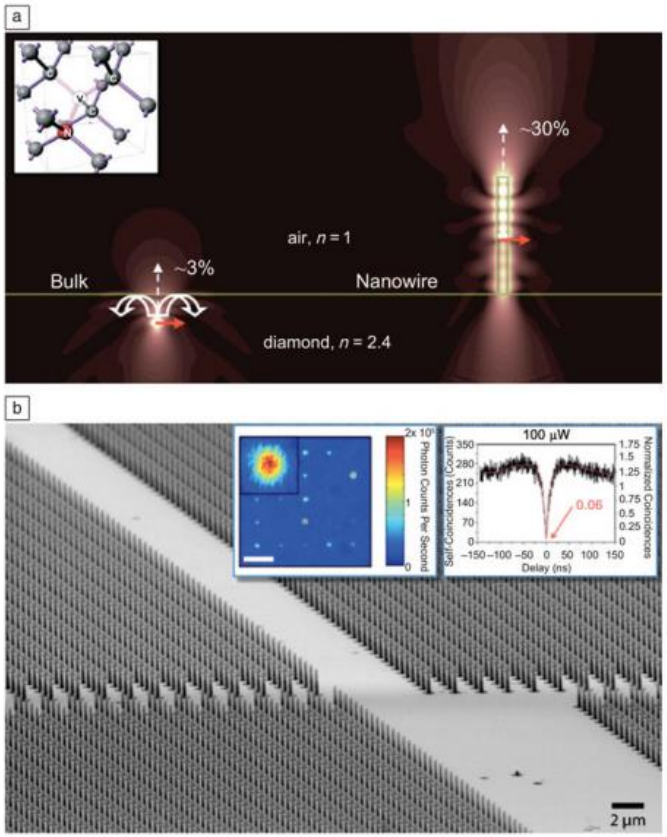

Faculty Groups:
Marco Loncar
Amir Yacoby
Mikhail Lukin
Hongkun Park

Figure 1. Diamond nanowires. (a) Emission profiles of a nitrogen vacancy (NV) embedded in bulk diamond crystal (left) and a diamond nanowire (right), obtained using finite-difference time-domain modeling. Position and orientation of the NV dipole is indicated by the red arrows. Collection efficiency for photons emitted by an NV (inset) in a bulk diamond crystal is low (~3%) due to the total internal reflection at the diamond-air interface. The collection efficiency can be increased 10 times (~30%) using diamond nanowires. *n*, refractive index. (b) Scanning electron microscopy image of diamond nanowires, ~2 μm tall and 200 nm in diameter, fabricated in single crystal diamond. Inset shows a confocal image of a 5 × 5 array of nanowires—each bright spot corresponds to a nanowire with a single NV center. Photon antibunching, indicative of single photon emission, is also shown for one of the nanowires (inset plot).

Marko Lončar and Andrei Faraon. 2013. "Quantum photonic networks in diamond." MRS Bulletin, 2, 38: 144-148.

Faraday Cage Angled Etch

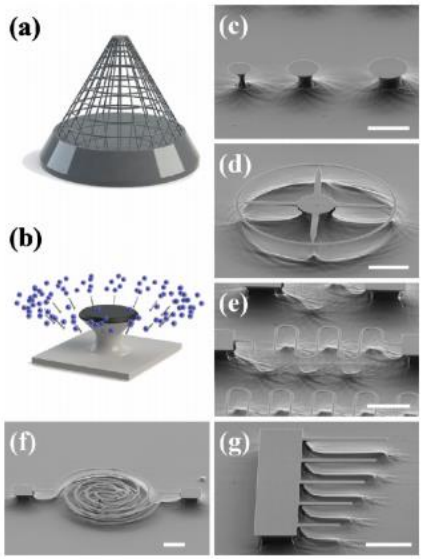

Figure 4. Schematic illustrations of (a) conical Faraday cage design and (b) angled-etching of the substrate from all directions. SEM images of (c) ~3–5 μm diameter undercut microdisks and (d) ~500 nm wide nanoring structure; (e) ~500 nm wide curved and (f) ~750 nm wide spiral nanobeams; and (g) ~1 μm wide nanobeam cantilevers. All SEM images were taken at a 60° stage tilt. Scale bars correspond to 5 μm.

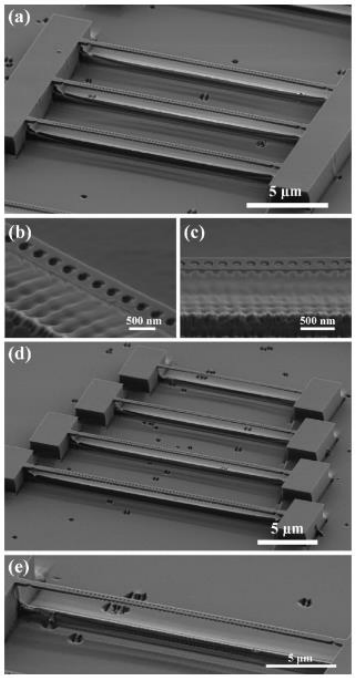

Figure 3. SEM images of (a) an array of fabricated diamond nanobeam cavity prototypes and (b–c) cavity region of an individual nanobeam cavity. (d) SEM image of an array of nanobeam cavities which are physically scaled from 75% to 135%, and (e) zoomed in image of smallest, 75% scaled nanobeam cavity in the array. All SEM images were taken at a 60° stage tilt.

Michael J Burek, Nathalie P de Leon, Brendan J Shields, Birgit JM Hausmann, Yiwen Chu, Qimin Quan, Alexander S Zibrov, Hongkun Park, Mikhail D. Lukin, and Marko Lončar. 2012. "**Free-standing mechanical and photonic nanostructures in single-crystal diamond**." Nano letters, 12: 6084-6089.

Diamond Angled-etching

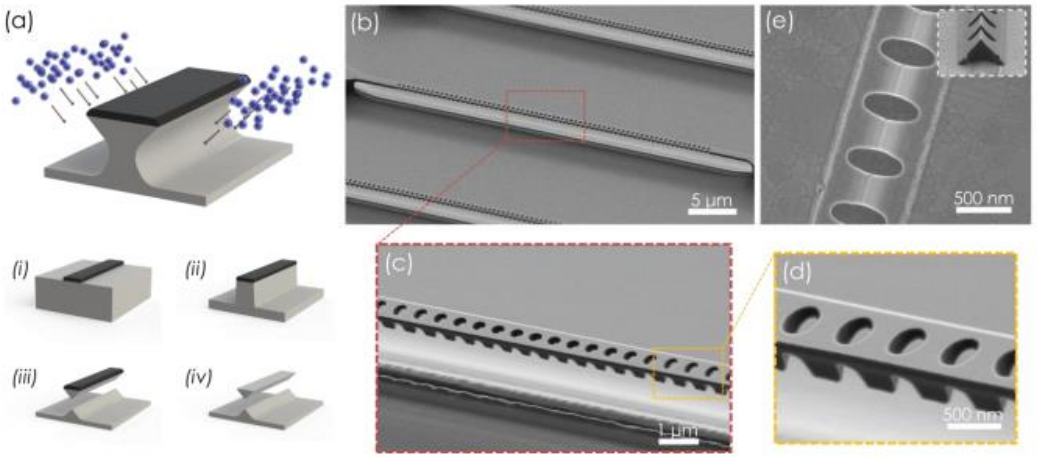

Figure 2 | Fabricated diamond optomechanical crystals. (a) Illustration of angled-etching used to realize diamond optomechanical crystals. Angled-etching nanofabrication steps: (i) define an etch mask on substrate via standard fabrication techniques, (ii) transfer etch mask pattern into the substrate by conventional top down plasma etching, (iii) employ angled-etching to realize suspended nanobeam structures (see illustration), (iv) remove residual etch mask. SEM images of **(b)** a fabricated diamond optomechanical crystal, **(c)** zoomed in view of the defect region, and **(d)** high-resolution image of fabricated air holes comprising the Bragg mirror region. **(e)** SEM image of an (inverted) diamond optomechanical crystal, liberated from the diamond substrate via stamping on a silver-coated silicon wafer. Inset shows a tilted (60°) SEM image of a broken diamond optomechanical crystal, revealing the triangular cross-section.

Michael J. Burek, Justin D. Cohen, Seán M. Meenehan, Thibaud Ruelle, Srujan Meesala, Jake Rochman, Haig A. Atikian, et al. 2015. "**Diamond optomechanical crystals**." arXiv:1512.04166.

Simulations of Faraday Cage Angled Etch

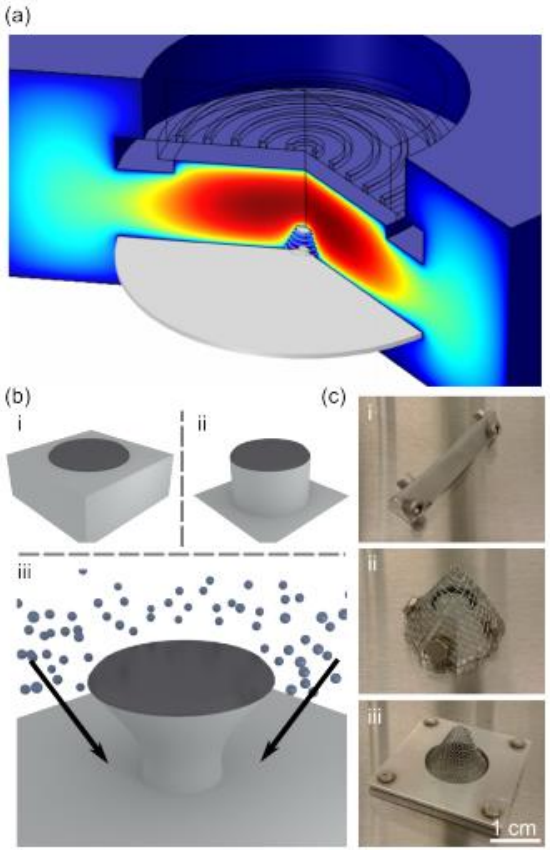

FIG. 1. (Color online) Overview of Faraday cage angled-etching (a) 3D simulation of reactor chamber with an argon plasma and a central Faraday cage (details in text). (b) Schematic of angled-etching. The ions, directed by the equipotential on the cage boundaries, are incident upon the sample at an angle. The etch mask defines the shape of the structure. (c) Examples of different cages used for angled-etching, including (i) a triangular cage with a fine mesh (ii) a wrapped cage with a coarse mesh and (iii) a molded cage with a medium mesh, with a shape maintained by retaining plates.

Pawel Latawiec, Michael J. Burek, Young-Ik Sohn, and Marko Loncar. 2016. "**Faraday cage angled-etching of nanostructures in bulk dielectrics**." Journal of Vacuum Science & Technology B, 34: 041801.

Simulations of Faraday Cage Angled Etch

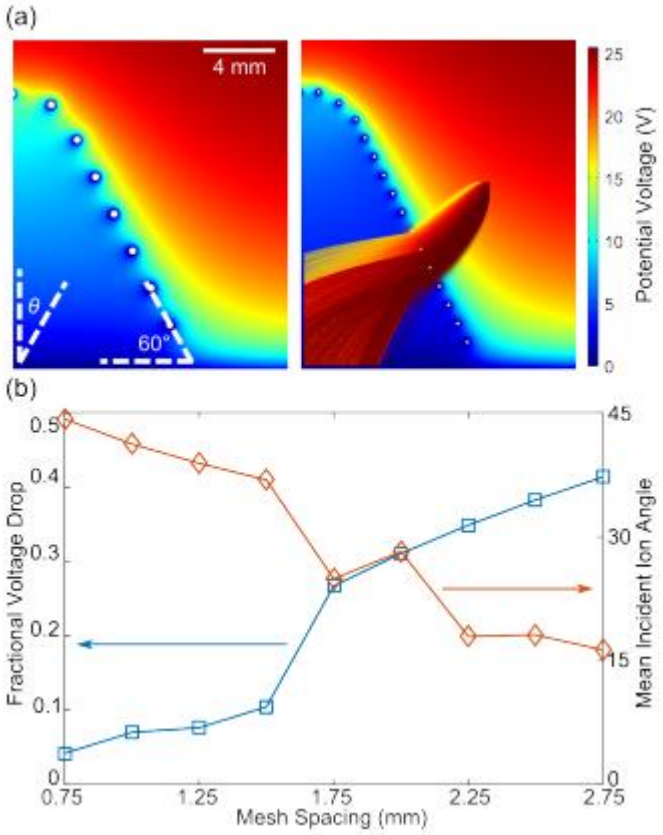

FIG. 3. (Color online) Simulated voltage drops inside the Faraday cage. (a) Simulated etching potentials for a coarse cage (left) and fine cage (right). The coarse cage has a larger potential gradient within, influencing the path the ion takes. The simulated ion trajectories from a single point outside the cage are overlayed on the right hand side, with coloring to provide visual contrast. All simulated cages have a cage angle of 60 degrees. (b) Voltage drop inside the cage relative to the etch potential (squares, left axis) and resultant mean incident ion etching angle, defined from the normal (diamonds, right axis).

Pawel Latawiec, Michael J. Burek, Young-Ik Sohn, and Marko Loncar. 2016. "**Faraday cage angled-etching of nanostructures in bulk dielectrics**." Journal of Vacuum Science & Technology B, 34: 041801.

Center for Nanoscale Systems Harvard University

More Diamond Devices by FCAE

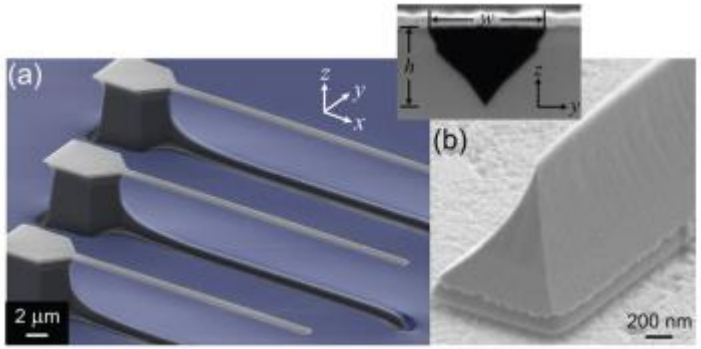

Zin Lin, Steven G Johnson, Alejandro W Rodriguez, and M. Loncar. 2015. "**Design of diamond microcavities for single photon frequency down-conversion**." Optics express, 19, 23: 25279-25294.

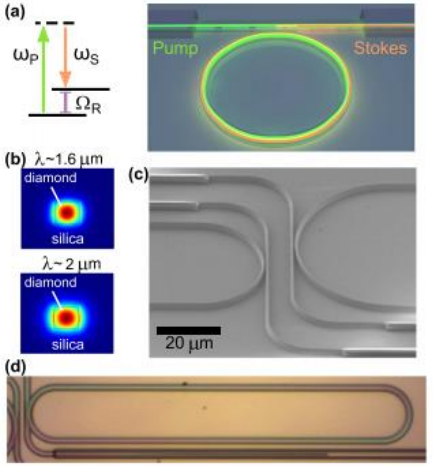

Fig. 1. Diamond-microresonator-based Raman laser design. (a) Energy level diagram of the Raman scattering process (left), wherein a high-energy pump photon with frequency ω_p is scattered into a lower frequency Stokes photon, ω_S, and an optical phonon, Ω_R (~40 THz in diamond). We pump with telecom lasers ($\lambda_p \sim 1.6$ µm) corresponding to $\omega_p \sim 190$ THz, resulting in a Stokes output at $\omega_S \sim 150$ THz, i.e., $\lambda_S \sim 2$ µm. A schematic illustrating the device principle (right) shows a pump wave (green) entering a high-Q microcavity, where it enables Stokes lasing (orange) via stimulated Raman scattering. (b) Simulated TE mode profiles of diamond waveguides with width 800 nm and height 700 nm fully embedded in silica, at the pump ($\lambda_p \sim 1.6$ µm, top) and Stokes ($\lambda_S \sim 2$ µm, bottom) wavelengths, showing good overlap. (c) Scanning-electron-microscopy image of the nanofabricated diamond racetrack resonators on a SiO_2-on-Si substrate before cladding with PECVD silica, showing the bus-waveguide-coupling region (gap ~500 nm) and transition to polymer (SU-8) waveguides for efficient coupling to lensed fibers. (d) Optical micrograph of a diamond racetrack microresonator with path length ~600 µm and bending radius ~20 µm, after a PECVD silica cladding layer is deposited on top.

Pawel Latawiec, Michael J. Burek, Young-Ik Sohn, and Marko Loncar. 2016. "**Faraday cage angled-etching of nanostructures in bulk dielectrics**." Journal of Vacuum Science & Technology B, 34: 041801.

A robust scanning diamond sensor for nanoscale imaging

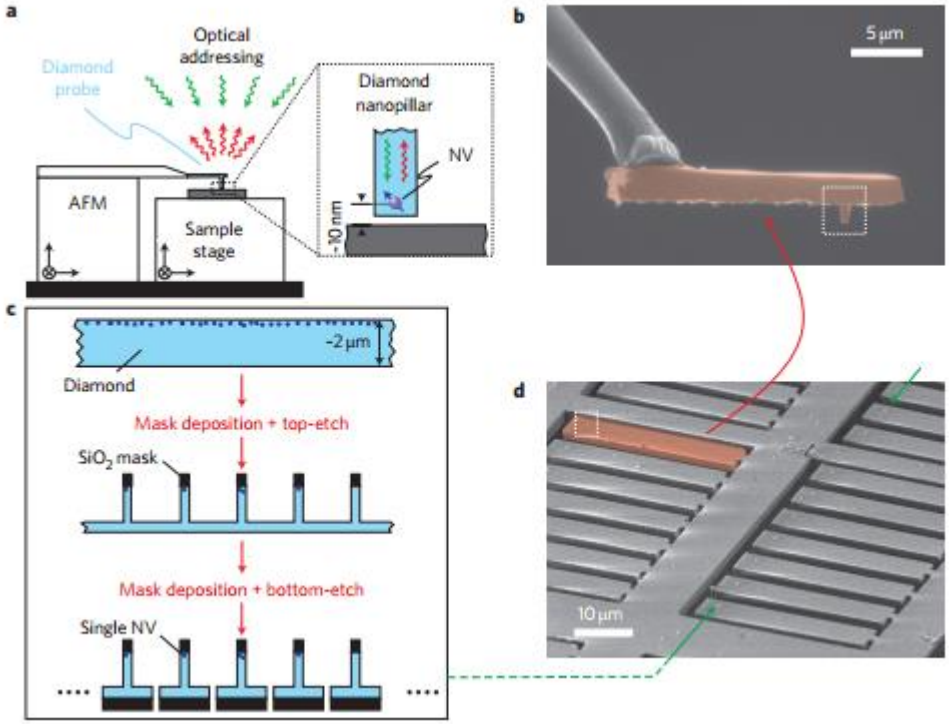

Figure 1 | Experimental set-up and probe fabrication for the scanning NV sensor. a, Schematic of the set-up, consisting of a combined optical and atomic force microscope (AFM). We use a 532 nm laser (green arrows) to address the scanning NV centre through its red fluorescence (red arrows). The scanning NV centre resides in a diamond nanopillar (inset) and its proximity to the sample is maintained by means of AFM feedback. **b**, SEM image of a single-crystalline diamond nanopillar probe (false colour coded in red) with a single NV centre in its tip (see Fig. 2). **c**, Brief depiction of the fabrication process for scanning single-crystalline diamond NV sensors. Electron-beam lithography is used to define nanopillars and platforms from the top and bottom sides of a few-micrometre thin diamond membrane. Patterns are then transferred to the diamond by reactive ion etching. **d**, SEM image of a finalized array of diamond platforms with nanopillars. In all panels, dotted rectangles highlight diamond nanopillars.

P. Maletinsky*, S. Hong*, M. S. Grinolds*, B. Hausmann, M. D. Lukin, R. L. Walsworth, M. Loncar, A. Yacoby "A robust scanning diamond sensor for nanoscale imaging with single nitrogen-vacancy centres" *Nature Nanotechnology* **7**, 320-324 (2012).

Center for Nanoscale Systems
Harvard University